Development of CuO coated ceramic hollow fiber membrane for peroxymonosulfate activation: a highly efficient singlet oxygen-dominated oxidation process for bisphenol a degradation

Songxue Wang[a], Jiayu Tian[a,b,*], Qiao Wang[a], Feng Xiao[c], Shanshan Gao[b], Wenxin Shi[d], Fuyi Cui[d,**]

[a] State Key Laboratory of Urban Water Resource and Environment, School of Environment, Harbin Institute of Technology, Harbin 150090, China
[b] School of Civil Engineering and Transportation, Hebei University of Technology, Tianjin 300401, China
[c] School of Renewable Energy, North China Electric Power University, Beijing 102206, China
[d] College of Urban Construction and Environmental Engineering, Chongqing University, Chongqing 400044, China

ABSTRACT

A CuO coated ceramic hollow fiber membrane with dual functionalities of membrane filtration and peroxymonosulfate (PMS) activation was successfully constructed by applying phase-inversion and dip-coating technologies. The CuO coating condition was investigated, and the optimized CuO coated ceramic hollow fiber membranes (CuO@CHFMs) exhibited excellent catalytic activity for PMS activation to deprecate bisphenol A (BPA) in the presence of humic acid (HA), chloride ions (Cl^-) and bicarbonate (HCO_3^-). Based on the scavenger experiments and electron paramagnetic resonance (EPR) analyses, the non-radical reactive oxygen species - singlet oxygen ($^1O_2$), rather than sulfate radicals ($SO_4^{\cdot-}$) or hydroxyl radicals ($^\cdot OH$), was elucidated as the primary reactive species responsible for the oxidation of BPA in the system. The redox circles of Cu(II)/Cu(I) on the CuO surface of the CuO@CHFMs are mainly responsible for PMS activation and a possible degradation pathway of BPA was proposed. Moreover, the CuO@CHFMs exhibited excellent stability and reusability without tedious catalyst separation/recovery processes. This study is meaningful for the development of novel catalytic membrane with PMS activation functionality in water treatment.

1. Introduction

Low-pressure membrane filtration, which includes microfiltration (MF) and ultrafiltration (UF), has become one of the most popular technology for drinking water treatment due to decreased operating cost, relative simplicity of installation, small footprint requirement and reliability in operation when compared with conventional treatment processes [1–3]. However, insufficient removal of dissolved organic matter, especially the toxic organic contaminants which pose a significant environmental and health concern are still a critical obstacle limiting its further widespread application [4–6]. As well known, advanced oxidation processes (AOPs) are considered to be excellent option for the removal of organic pollutants in water, owing to the generation of highly reactive oxygen species (ROS) such as hydroxyl radicals ($^\cdot OH$) and superoxide radical ($O_2^{\cdot-}$) [7–11]. Therefore, a promising strategy to increase the removal efficiency of organic contaminants during low-pressure membrane filtration is the combination with AOPs. To date, heterogeneous AOPs are usually used as the pre-treatment process to the water feeding the membrane filtration modules, or as the post-treatment process to the retentate effluent of the membranes [12,13]. In the former case, the permeate flux of membrane is compromised due to the stacking and accumulation of catalyst nanoparticles on the membrane surface; whereas in the latter case, an additional treatment is necessary to separate and recover the catalyst particles at the end of the treatment [14–16].

More recently, some researchers began to immobilize heterogeneous catalysts on the membrane support to produce a novel catalytic membrane with dual functionalities of membrane filtration and advanced oxidation [17–21]. The catalytic membrane system can not only eliminate the adverse effect of catalyst on membrane permeability but

also avoid the difficulty of catalyst separation and recovery [22–27]. For example, Paredes and co-workers immobilized TiO_2 on polyvinylidene fluoride dual layer membrane to improve the photocatalytic removal of pharmaceuticals in different water matrices [28]. Cheng and co-workers fabricated Mn oxide incorporated membrane to enhance the catalytic ozonation of p-chloronitrobenzene [29]. Nevertheless, photocatalytic water treatment is easily influenced by water quality, weather and other conditions in practical application, and the ozone-based technology requires a sophisticated ozone generation and waste gas destruction system, which are not conducive to the further development and application of catalytic membrane [30]. Among various AOPs, Peroxymonosulfate (PMS) activation has recently emerged as a convenient and efficient process for removing refractory organic contaminants in water due to their mild reaction conditions, superior oxidation ability, and avoidance of secondary pollution of sludge [31–34]. Meanwhile, PMS can be activated efficiently by various transition metal (such as Cu, Mn, Fe or Co) oxides, which makes it possible to prepare the metal oxide coated ceramic membrane with excellent capability for PMS activation [35–37]. In addition, ceramic hollow fiber membrane (CHFM) is regarded as a promising catalytic membrane support because of its self-supporting structure, high surface area, better chemical and mechanical stabilities [38–40]. Therefore, the combined catalytic CHFM filtration/PMS activation system would have great potentials to be implemented as an effective treatment of the water containing recalcitrant organics pollutants.

Herein, the CuO coated ceramic hollow fiber membranes (CuO@CHFMs) were prepared via phase-inversion and dip-coating methods, with the expectation to incorporate both the functions of PMS activation and membrane filtration in one process. The morphologies and properties of the CuO@CHFMs were systematically characterized. Bisphenol A (BPA) was chosen as the model contaminant to evaluate the catalytic performance of the CuO@CHFMs. Effect of operation parameters and water matrix species on BPA removal in the CuO@CHFMs/PMS system were assessed. Furthermore, the ROS responsible for the oxidation of BPA in the system were investigated via a series of experiments and instrument characterization, and a possible degradation pathway of BPA was proposed. Finally, the stability and reusability of the CuO@CHFMs were also evaluated.

2. Materials and methods

2.1. Reagents

Aluminium oxide (Al_2O_3), copper oxide (CuO) and titanium oxide (TiO_2) powders were obtained from Xuancheng Jingrui New Material Co., Ltd., China. Polysulfone (PSf) was purchased from Solvay SA, Belgium. N,N-dimethylacetamide (DMAC), Polyvinylpyrrolidone (PVP, k-30), copper nitrate trihydrate ($Cu(NO_3)_2 \cdot 3H_2O$) and polyethylene glycol (PEG, MW = 4000) were obtained from Xilong Scientific Co., Ltd., China. Potassium peroxymonosulfate (PMS, $KHSO_5 \cdot 0.5KHSO_4 \cdot 0.5K_2SO_4$), 2,2,6,6-tetramethyl-4-piperidinol (TEMP) and 5,5-dimethyl-1-pyrolin-Noxide (DMPO) were purchased from Sigma-Aldrich Co., Ltd., USA. Bisphenol A (BPA), Ethanol, methanol (MeOH), butyl alcohol (TBA), Furfuryl alcohol (FFA), sodium bicarbonate ($NaHCO_3$), humic acid (HA), sodium hydroxide (NaOH) and hydrochloric acid (HCl) were obtained from Aladdin Chemistry Co., Ltd., China. All solutions were prepared using deionized (DI) water.

2.2. Preparation of ceramic hollow fiber membrane

The ceramic hollow fiber membrane was fabricated using a phase-inversion process followed by sintering. The detailed preparation procedures were described elsewhere [41]. The spinning suspension was composed of 41.25 wt% Al_2O_3, 2 wt% TiO_2, 6.5 wt% PSf, 49.75 wt% DMAC and 0.5 wt% PVP. The pressure of the spinning process was maintained at 0.02 MPa and the temperature was kept at 25 $\pm$ 0.5 °C.

The as-spun hollow fibers emerging from the spinneret (outer diameter: 3.0 mm, inner diameter: 1.2 mm) passed through an air gap of 2 cm and were soaked in tap water for 24 h for complete gelation. The dried hollow fiber precursors were calcined at 1550 °C for 3 h at the static air atmosphere.

2.3. Preparation of CuO coated ceramic hollow fiber membrane

The CuO coated ceramic hollow fiber membrane was prepared via the dip-coating method followed by calcination. 1 g PEG was added to 25 mL ethanol with vigorous magnetic-stirring for 20 min at 60 °C. After cooling to ambient temperature, 5 g $Cu(NO_3)_2 \cdot 3H_2O$ was added to the above solution with vigorous stirring for 60 min to form a homogeneous blue solution, obtaining the CuO coating solution. The as-prepared ceramic hollow fiber membrane was immediately dipped into the CuO coating solution for 5 min, then removed from the solution at a speed of 0.5 mm/s. The excess solution was drained by the filter papers and then dried at 60 °C for 6 h. Finally, the coated hollow fiber membrane was calcined at 400–800 °C for 3 h in a muffle furnace. After that, the CuO coated hollow fiber membrane was washed with pure water for several times and dried at 60 °C in a vacuum oven for 2 h. These steps were repeated 1–3 times. The resultant black CuO coated hollow fiber membranes were denoted as CuO@CHFMs-X-Y, where X and Y stand for the calcination temperature and coating times, respectively.

2.4. Characterization

The crystal phase and material composition of the membrane samples were characterized by a X-ray diffractometry (XRD) (D8 Advance, Bruker Corporation, Germany) with Cu Ka radiation (λ = 0.15418 nm). The morphologies of the membrane were observed by a field emission scanning electron microscopy (FE-SEM) (SIGMA500, Zeiss, Germany). The mean pore size and pore size distribution of the membrane were determined by Mercury porosimetry (Micrometrics AutoPore9510, USA). The generated ROS were investigated by Electron spin resonance (ESR) spectroscopy (Bruker A300 spectrometer, Germany). X-ray photoelectron spectroscopy (XPS) analyses were conducted using a photoelectron spectrometer (ESCALAB 250Xi, Thermo Scientific, USA) equipped with a monochromatic Al Kα excitation source.

The water flux was measured to evaluate the membrane permeation property using a lab-scale cross-flow setup (Fig. S1). Before measurement, the membranes were pre-pressurized under 0.2 MPa for 30 min to reach a stable state. The permeate flux F ($L \cdot m^{-2} \ h^{-1} \ bar^{-1}$) of the ceramic hollow fiber membrane was calculated by the following Eq. (1):

$$F = \frac{V}{A \cdot t \cdot \Delta P} \tag{1}$$

where V (L) is the permeate volume, A (m^2) is the effective area of membrane module, t (h) is the operation time and ΔP (bar) is the transmembrane pressure.

2.5. Experimental procedures

The catalytic activity of CuO@CHFMs was investigated by the cross-flow filtration apparatus as shown in Fig. S1. The feed tank had a working volume of 500 mL and was equipped with water bath for controlling temperature. The membrane module was composed of 4 ceramic hollow fibers and the effective membrane area was ˜15 cm². Batch experiments were conducted with a 10 mg/L BPA solution and a PMS concentration of 0.5 mM and the water temperature was kept constant at 25 °C. The pH of the feed solution was adjusted by 1.0 M NaOH or H_2SO_4 solution. The feed solution was forced to flow through the membrane module by a pump. The membrane filtration (outside-in mode) was carried out in a cross-flow manner and the permeate flux was controlled by adjusting the pressure of the system. 1 mL of water sample was collected from the permeate at desired time intervals and
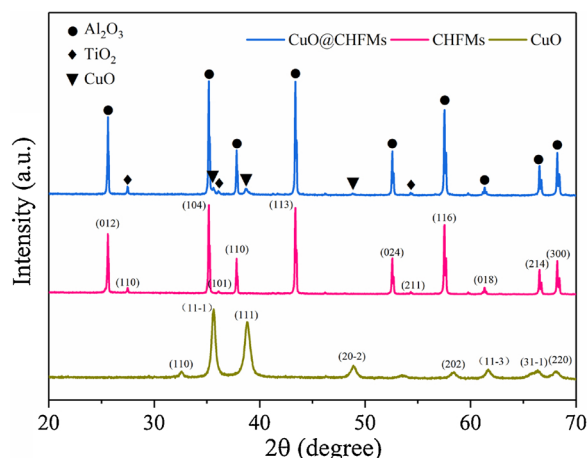
Fig. 1. XRD patterns of CuO, CHFMs and CuO@CHFMs.

filtered through 0.22 μm membranes, then 0.5 mL of 1 M sodium thio-sulfate solution was injected into the filtered solution as a quenching reagent. The concentration of BPA was detected by the HPLC system (Waters Baseline 810) equipped with a Supelcosil LC-18-DB column (250 mm × 4.6 mm) and a Waters 486 tunable UV absorbance detector. The mobile phase was composed of water and methanol with a volume ratio of 40 : 60 at a flow rate of 1 mL/min. The leaching concentration of copper ions in aqueous solution was analyzed by an inductively coupled plasma optical emission spectrometry (ICP-OES) (Optima 5300DV, Perkin Elmer, USA). Total organic carbon (TOC) was measured by a TOC analyzer (multi N/C 2100S, Analytik Jena, Germany). Degradation intermediates and products of BPA were analyzed by an ultra-performance liquid chromatography/MS/MS (Acquity UPLC, XEVO TQ MS) with a triple quadrupole detector (Xevo TQ-S) at ESI negative ionization mode.

3. Results and discussion

3.1. Structure and morphology

XRD patterns of CuO, CHFMs and CuO@CHFMs are shown in Fig. 1. The major peaks at 25.6° (012), 35.1° (104), 43.4° (113) and 57.5° (116) were well indexed as the standard diffraction patterns of rhombohedral Al_2O_3 (PDF#10-0173) and the diffraction peaks located at 27.5° (110), 36.1° (101) and 54.3° (211) corresponding to tetragonal TiO_2 (PDF#65–0190), indicating that CHFMs consists of Al_2O_3 and TiO_2 after calcination. In comparison with CHFMs, the CuO@CHFMs specimens showed the peaks at 35.5° (11-1), 38.7° (111) and 48.7° (20-2), corresponding to monoclinic CuO (PDF#48-1548). The result displayed a highly crystalline and single-phase structure of CuO coated on CHFMs and without any peaks of unreacted precursors.

The morphologies of CuO@CHFMs sintered at different temperatures and coated with different times are shown in Fig. 2. Fig. 2a–d show that the particle size of CuO on the outer surface of the CuO@CHFMs increased with the increase of sintering temperature from 400 °C to 800 °C. As illustrated in Fig. 2e–l, the coating thickness of CuO layer on the outer surface increased obviously with the increase of coating times. When only one-time coating was conducted, the CuO layer thickness was only 0.6 μm, and the coating layer cannot completely cover the outer surface of the substrate membrane. When the membrane was coated with 2 times, the coating layer thickness was increased to 1.0 μm and the outer surface of the membrane exhibited uniform morphologies and generally no defect. When the membrane was further coated with 3 times, the coating thickness reached to 2.0 μm. Howerver, some huge cracks appeared in the coating layer due to multiple sintering. The EDX elemental mapping conducted for the CuO@CHFMs-500-2 (Fig. S2) further demonstrated that the CuO was

distributed homogeneously on the outer surface of the membrane. Therefore, it was considered that two-time coating might be an optimum for the preparation of CuO@CHFMs.

3.2. Porosity and permeability

The mean pore size and porosity of the CuO@CHFMs sintered at different temperatures and coated with different times are presented in Fig. 3a and b. As compared with the uncoated membrane, the mean pore size of CuO@CHFMs-400-1 decreased dramatically from 679 nm to 368 nm, because the large pore on the support membrane surface was effectively covered by the CuO coated layer. With the increase of sintering temperature from 400 °C to 800 °C, the mean pore size exhibited a slight decrease due to the growth of CuO particles on the membrane surface. Meanwhile, with the increase of CuO coating times, the mean pore size was also shown to be decreased remarkably (~200 nm with 3 coating times). On the other hand, the porosity was observed to be less influenced by sintering temperature and the CuO coating times, indicating the coated CuO was mainly retained on the membrane surface, and almost would not block the membrane pores. In addition, the pore size distribution curves of the CuO@CHFMs were also obtained, as shown in Fig. 3c and d. The results indicated that increasing coated times was more effective to reduce the membrane pore size in comparison of increasing sintering temperature.

Fig. 4 exhibits the pure water flux for the CuO@CHFMs sintered at different temperatures and coated with different times. The fluxes of CuO@CHFMs were shown to be lower than the uncoated ceramic hollow fiber membrane, possibly due to the coated CuO layer on the membrane surface increased the filtration resistance for the water to permeate. The flux decreased slightly with the increase of sintering temperature, while decreased significantly with the increase of coating times, suggesting that compared to increasing sintering temperature, increasing coating times has a more significant effect on the membrane flux.

### 3.3. PMS activation by CuO@CHFMs for BPA degradation

BPA was used as the target contaminant to evaluate the catalytic performance of CuO@CHFMs. The widespread use of BPA in consumer products and the lack of effective treatment have led to its ubiquitous existence in surface waters, which has posed a risk to the aquatic lives and other life-forms through consumption of the contaminated water [42–45]. As shown in Fig. 5, the CuO@CHFMs-400-1 exhibited a negligible adsorption for BPA, and PMS alone degraded less than 5% of BPA in 30 min. On the contrary, as high as 91.4% of BPA degradation was achieved by the CuO@CHFMs-400-1/PMS system. Meanwhile, the degradation efficiency of BPA in the uncoated CHFMs/PMS system was shown to be only 7.6%, demonstrating the excellent catalytic performance of CuO@CHFMs for PMS activation. To rule out the possibility that the high catalytic activity was caused by the leaching of CuO from the coated membrane, the effect of copper ions (1 g/L) on the BPA degradation was evaluated in a homogeneous process. Under the same operating conditions, the degradation efficiency of BPA after 30 min reaction was only 5.8%, implying that the high catalytic activity for PMS activation and BPA degradation could be majorly attributed to the CuO layer coated on the CHFMs.

The effect of sintering temperature on the catalytic activity and Cu leaching of the CuO@CHFMs were investigated and the results are shown in Fig. 6a. It was found that the degradation rate of BPA decreased slightly from 91.4% to 87.6% as the sintering temperature increased from 400 °C to 500 °C, while the degradation rate sharply decreased to 67.2% and 53.7% when the sintering temperature further increased to 600 °C and 800 °C, respectively. This might be attributed to that the CuO in the coated layer sintered at low temperature possessed a small particle size with a high surface area (according to Fig. 2a–d and Fig. S3, low sintering temperature led to small size of CuO particles),
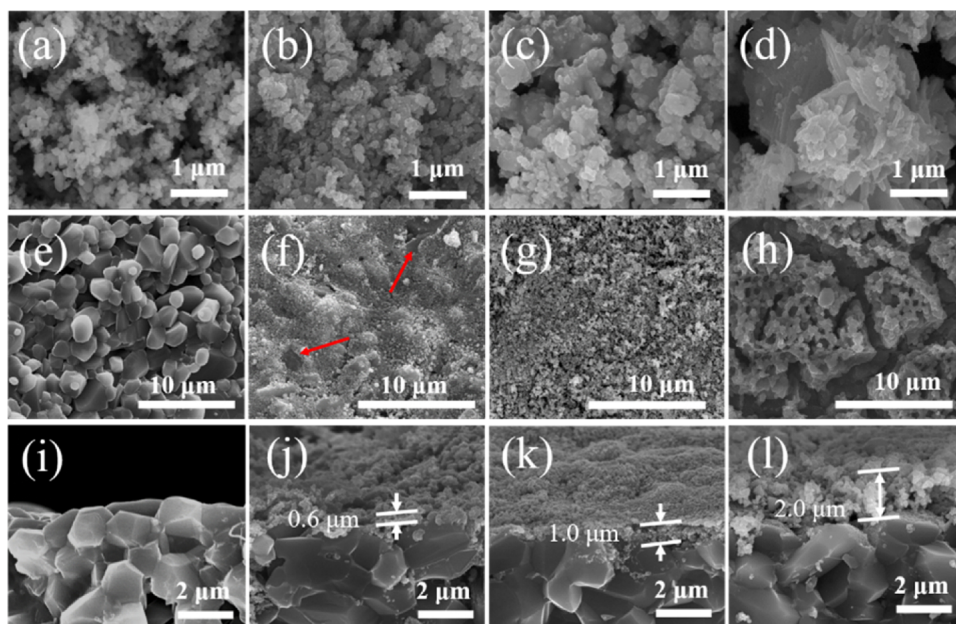
Fig. 2. SEM images of (a) CuO@CHFMs-400-1, (b) CuO@CHFMs-500-1, (c) CuO@CHFMs-600-1 and (d) CuO@CHFMs-800-1; outer surface SEM images of (e) CHFMs, (f) CuO@CHFMs-500-1, (g) CuO@CHFMs-500-2 and (h) CuO@CHFMs-500-3; cross-section SEM images of (i) CHFMs, (j) CuO@CHFMs-500-1, (k) CuO@CHFMs-500-2 and (l) CuO@CHFMs-500-3.
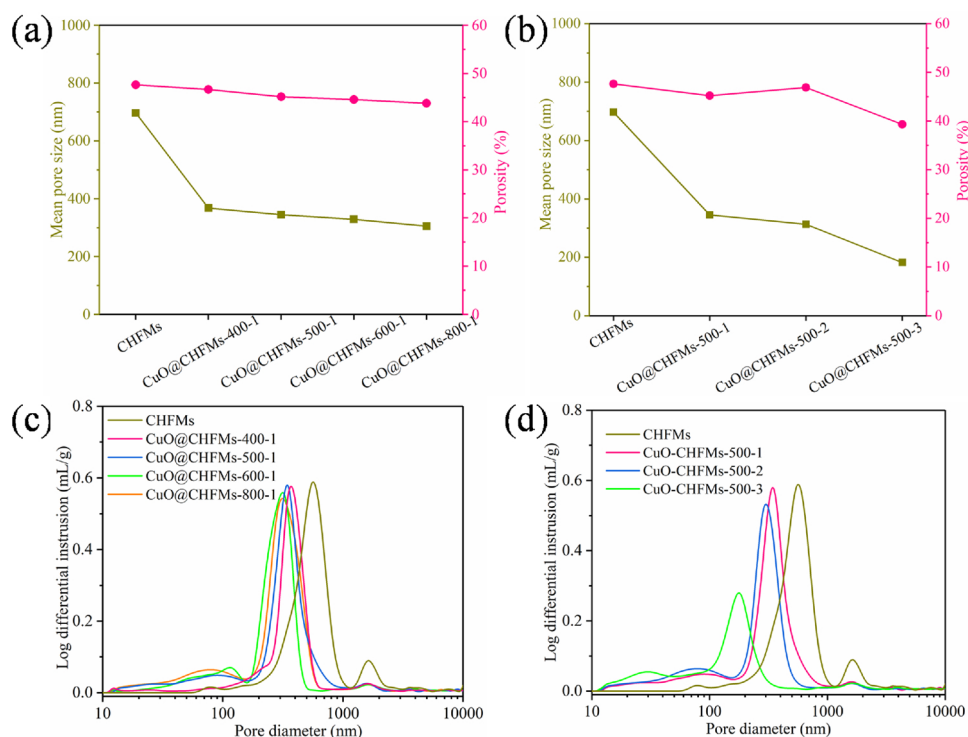
Fig. 3. Mean pore size and porosity of CuO@CHFMs sintered at different temperatures (a) and coated with different times (b); pore size distribution of CuO@CHFMs sintered at different temperatures (c) and coated with different times (d).

which can generate more active sites for the activation of PMS and subsequent degradation of BPA. However, the Cu leaching of the membrane with low sintering temperature is shown to be severer than that with high sintering temperature in the membrane/PMS system, might be due to that high sintering temperature can enhanced the stability of CuO on the coated membrane, at the cost of decrease of catalytic activity. Fig. 6b shows the effect of coating times on the catalytic activity and Cu leaching of the CuO@CHFMs. The degradation rates of BPA in the CuO@CHFMs-500-1, CuO@CHFMs-500-2 and CuO@CHFMs-500-3/PMS systems were 87.6%, 96.3% and 97.1%, respectively, indicating that increasing CuO coating times can improve the catalytic activity of the membrane, due to the higher amount of CuO

on the catalytic layer. Further, the Cu leaching was basically identical and kept less than 0.12 mg/L for the different coating times. In view of the lowest permeate flux of CuO@CHFMs-500-3 (as shown in Fig. 4b), CuO@CHFMs-500-2 with high catalytic activity and negligible Cu leaching was chosen as the optimal candidate in the following experiments.

3.4. Impact factors on the degradation of BPA

3.4.1. Influence of experimental conditions

Experiments were performed to investigate the BPA degradation efficiency in the CuO@CHFMs-500-2/PMS system under different
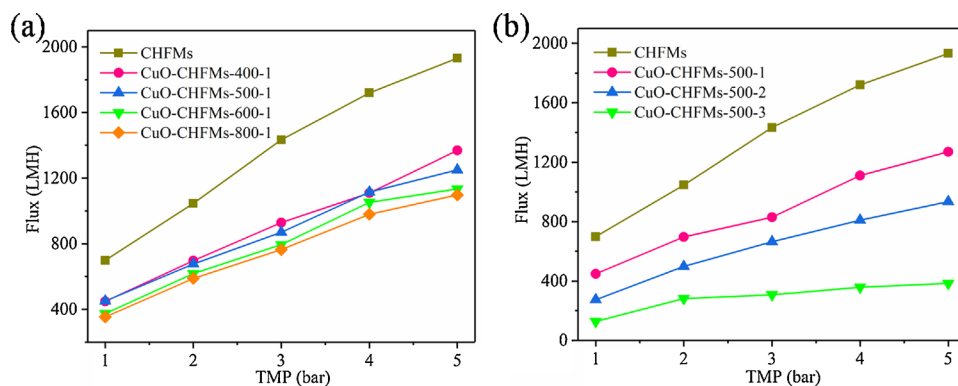
Fig. 4. Pure water flux under various TMPs for CuO@CHFMs sintered at different temperatures (a) and coated with different times (b).
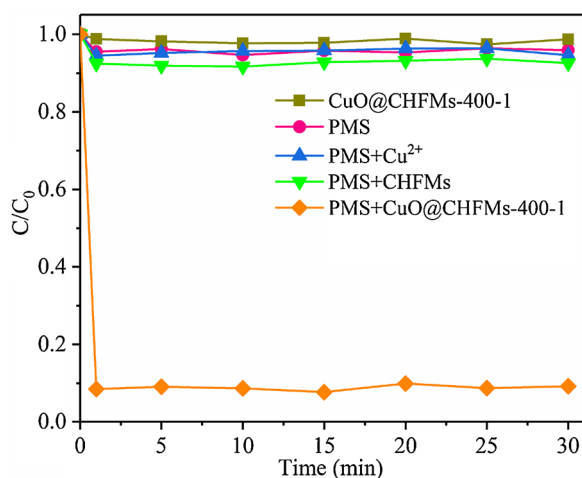

Fig. 5. BPA removal by CuO@CHFMs-400-1 adsorption, PMS, PMS/Cu^{2+}, PMS/CuO@CHFMs and PMS/CuO@CHFMs-400-1 ([PMS]$_0$ = 0.5 mM, [BPA]$_0$ = 10 mg/L, Flux = 70 LMH, pH = 7, T = 25 °C).

conditions. As presented in Fig. 7a, when the permeate flux was increased from 40 LMH to 200 LMH, the removal efficiency of BPA decreased from 98.2% to 83.4%. High permeate flux decreased the residence time of both BPA and PMS within the membrane, resulting in the decrease of BPA degradation rate. As shown in Fig. 7b, the degradation efficiency of BPA dropped gradually as the BPA concentration increased, and the degradation efficiencies of 98.5%, 96.3%, 93.2%, 85.8% and 65.6% were achieved at the initial BPA concentrations of 5, 10, 20, 50, and 100 mg/L, respectively. Fig. 7c displays that BPA degradation efficiency increased markedly from 53.0% to 96.3% as the

PMS dosage increased from 0.02 to 0.5 mM. However, in the CuO@CHFMs-500-2/PMS system, a further increase of the PMS dosage to 1.0 mM did not increase the BPA removal obviously, probably owing to the limited opportunities for PMS to interact with the CuO catalysts coated on the membrane.

3.4.2. Influence of NOM

NOM is ubiquitously present in drinking water sources and cannot be fully removed by conventional water treatment processes. NOM in water usually acts as a radical scavenger and may consume a large amount of SO$_4^{\bullet-}$ and ˙OH. NOM may also be adsorbed onto the catalyst surface and block reactive sites [46]. Humic acid (HA) as one of the typical NOM fractions was taken into account in the BPA degradation in the CuO@CHFMs-500-2/PMS system. As shown in Fig. 8, it was interesting to observe that there was essentially no significant influence when HA concentration ranging from 5 to 50 mg/L and the degradation rate of BPA was well kept at higher than 90% in the system. While in the CuO particle/PMS system (the CuO particle was obtained by calcining the CuO coating solution via the same process), the degradation rate of BPA decreased from 78.1% to 31.4% with the increase of HA concentration from 5 to 50 mg/L. The results indicated that the CuO@CHFMs-500-2/ PMS system could effectively eliminate the adverse effect of HA on BPA degradation. This was mainly attributed to the superior separation performance of the catalytic membrane. As shown in Fig. 8a, the CuO coated membrane possessed excellent rejection performance for HA (˜90%), suggesting that most of the HA molecules can be retained on the surface of the CuO coated layer. The degradation process of BPA might have occurred mainly in the pore channels of the catalytic membrane when BPA passing through the catalyst layer, and thus the HA exhibited a negligible influence on BPA degradation. Therefore, the influence of HA in the catalytic membrane/PMS system was much less than that in the traditional catalyst particle/PMS system.
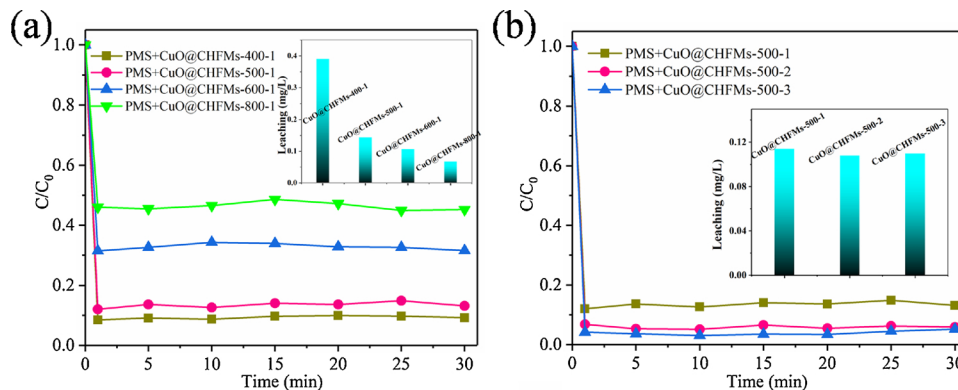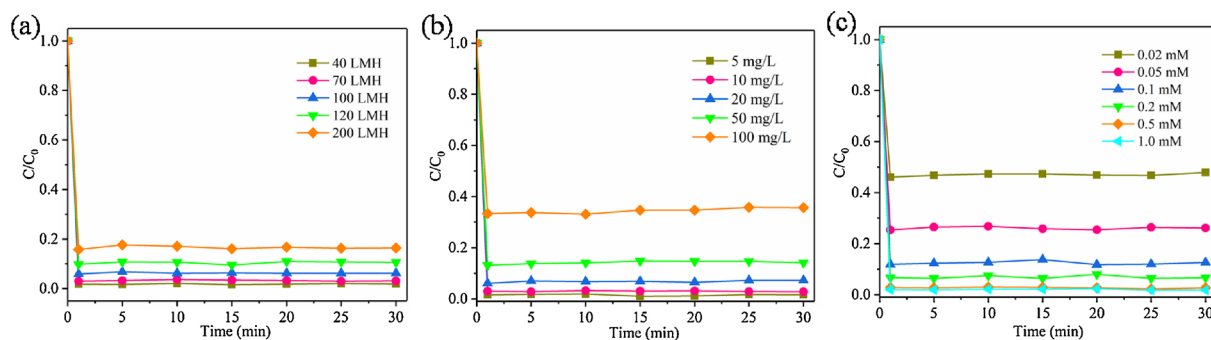

Fig. 6. Effect of sintering temperature (a) and coationg times (b) on the catalytic activity and leached Cu^{2+} concentration of the CuO@CHFMs ([PMS]$_0$ = 0.5 mM, [BPA]$_0$ = 10 mg/L, Flux = 70 LMH, pH = 7, T = 25 °C).

Fig. 7. (a) Effect of permeate flux on BPA degradation ($[PMS]_0 = 0.5\,mM$, $[BPA]_0 = 10\,mg/L$, pH = 7, T = 25 °C), (b) effect of BPA dose on BPA degradation ($[PMS]_0 = 0.5\,mM$, Flux = 70 LMH, pH = 7, T = 25 °C) and (c) effect of PMS dose on BPA degradation ($[BPA]_0 = 10\,mg/L$, Flux = 70 LMH, pH = 7, T = 25 °C).

3.4.3. Influence of inorganic ions

Chloride ions (Cl^-) and HCO_3^- are omnipresent in natural waters. Traditionally, Cl^- and HCO_3^- are believed to have a negative effect on AOPs, as both of them are regarded as radical scavengers [47]. HCO_3^- can react with $SO_4^{\bullet-}$ or $^{\bullet}OH$ to form a low reactive radical $CO_3^{\bullet-}$ (1.6 V) [46,48] and the oxidation of Cl- by $SO_4^{\bullet-}$ or $^{\bullet}OH$ in aqueous solution is known to produce several reactive species such as Cl_2 (1.36 V) and $Cl_2^{\bullet-}$ (2.09 V) [24], which is also less reactive and more selective than $SO_4^{\bullet-}$ (2.5–3.1 V) and $^{\bullet}OH$ (1.9–2.7 V) [49,50]. Taking into account the potential application of the CuO@CHFMs/PMS system in practical water treatment, the effect of Cl^- and HCO_3^- on BPA degradation in the CuO@CHFMs-500-2/PMS system was investigated. Unexpectedly, as presented in Fig. 9, the addition of 10 mM Cl^- and HCO_3^- displayed no obvious influence on the degradation of BPA, suggesting that $SO_4^{\bullet-}$ and $^{\bullet}OH$ might not be the major reactive species responsible for BPA degradation in the CuO@CHFMs-500-2/PMS system, as discussed in detail in the next section.

3.5. Catalytic oxidation mechanism

To clarify the major ROS for BPA degradation in the CuO@CHFMs-500-2/PMS system, a series of radical scavenging experiments were carried out with MeOH and TBA. MeOH is used to indicate the generation of $SO_4^{\bullet-}$ and $^{\bullet}OH$ with the high rate constants of 1.2–2.8×10^9 $M^{-1}\,s^{-1}$ and 1.6–7.7×10^7 $M^{-1}\,s^{-1}$, respectively [8], while TBA is used to scavenge $^{\bullet}OH$ with the reaction rate constant of 3.8–7.6×10^8 $M^{-1}s^{-1}$ [51]. As shown in Fig. 10a, upon the addition of excess MeOH and TBA, the degradation efficiency of BPA declined slightly from 96.3% to 85.6% and 88.1%, respectively, indicating that only a small amount of $SO_4^{\bullet-}$ and $^{\bullet}OH$ were generated in the CuO@CHFMs-500-2/PMS system, and the $SO_4^{\bullet-}$ and $^{\bullet}OH$ were not the dominant species responsible for BPA degradation in the system. Moreover, $O_2^{\bullet-}$ has limited reaction activity with electron-rich centers because of its anionic charge, which can hardly oxidize the target pollutant BPA [48]. In some previous studies [52–54], the singlet oxygen ($^1O_2$) and PMS direct oxidation has
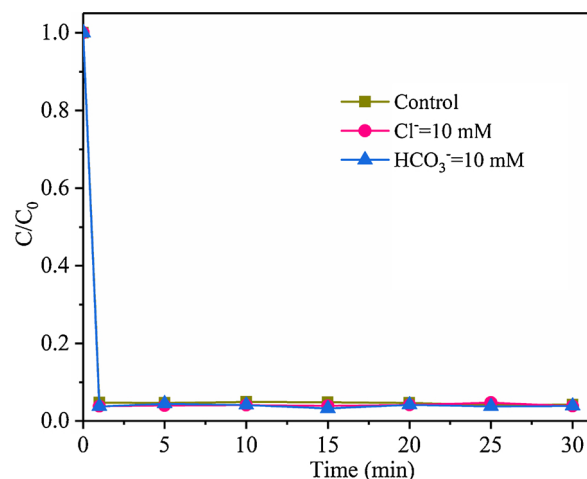
Fig. 9. Influence of Cl^- and HCO_3^- on BPA degradation in the CuO@CHFMs-500-2/PMS system ($[PMS]_0 = 0.5\,mM$, $[BPA]_0 = 10\,mg/L$, Flux = 70 LMH, pH = 7, T = 25 °C).

been identified as the main non-radical oxidation mechanisms in PMS activation processes. However, it has been demonstraed in Fig. 5 that PMS direct oxidation can hardly degrade BPA in the water. Therefore, it is supposed that $^1O_2$ was the dominant reactive oxygen species in the CuO@CHFMs-500-2/PMS system responsible for BPA degradation.

Furfuryl alcohol (FFA) has the reaction rate constant of 1.2×10^8 $M^{-1}\,s^{-1}$ with $^1O_2$, which was generally used as the scavenger to confirm the presence of $^1O_2$. However, a previous study indicated that FFA is a reducing agent which may react with PMS directly [55,56]. Fig. S4 shows that when FFA (10 mM) was adding to the feed, the reaction between FFA and PMS in the feed was relatively slow and the concentration of PMS only decreased to ~0.3 mM after 30 min. In the permeate, the concentration of FFA was almost the same as that in the
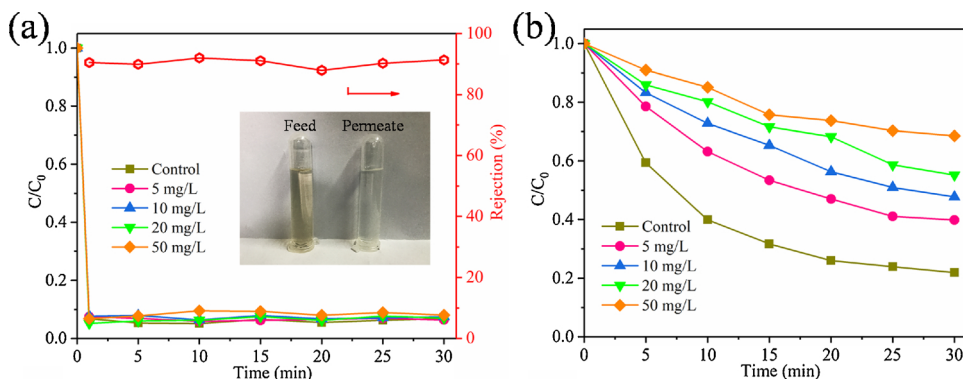
Fig. 8. (a) Effect of HA concentration on BPA degradation ($[PMS]_0 = 0.5\,mM$, $[BPA]_0 = 10\,mg/L$, Flux = 70 LMH, pH = 7, T = 25 °C) and HA rejection ($[HA] = 10\,mg/L$) in the system, (b) effect of HA concentration on BPA degradation in the CuO particle/PMS systems ($[PMS]_0 = 0.5\,mM$, $[BPA]_0 = 10\,mg/L$, $[CuO]_0 = 0.1\,g/L$, pH = 7, T = 25 °C).
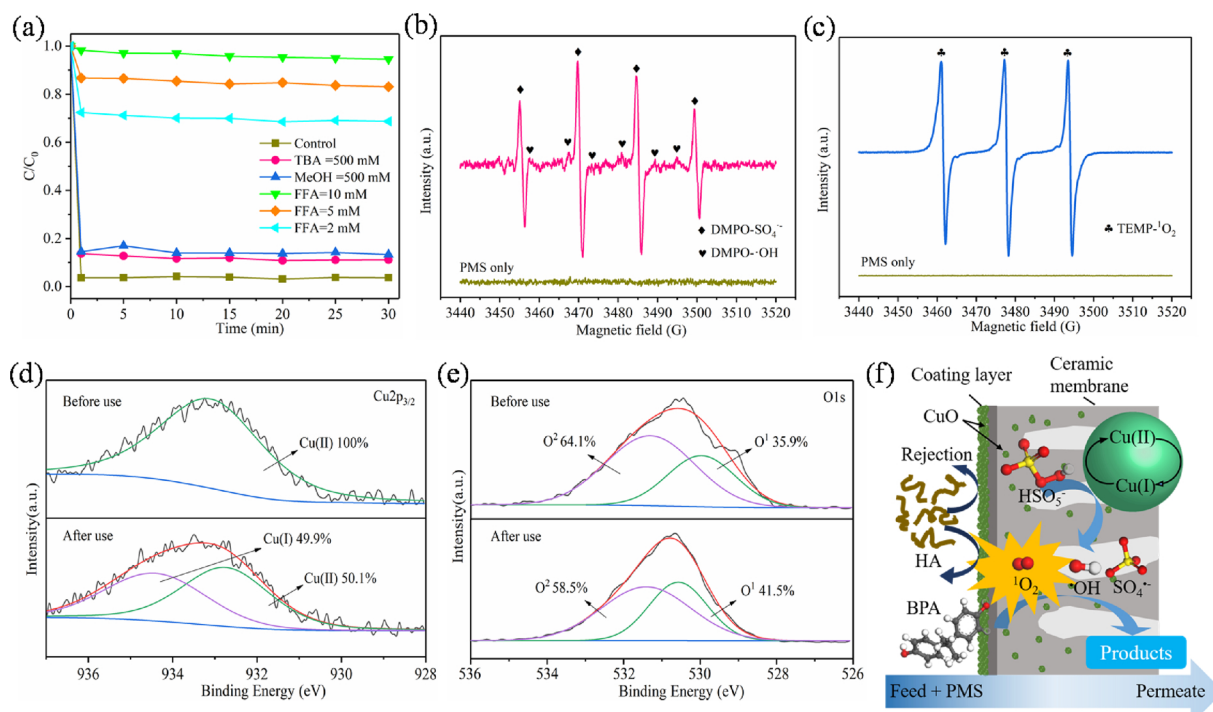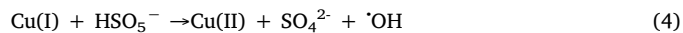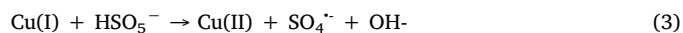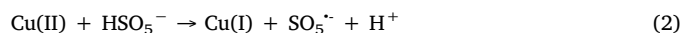
Fig. 10. (a) Effects of MeOH, TBA and FFA dosage on the degradation of BPA in the CuO@CHFMs/PMS system, (b) DMPO and (c) TEMP spin-trapping EPR spectra of PMS and CuO/PMS system ([PMS]$_0$ = 0.5 mM, [DMPO] = 10 mM, [TEMP] = 20 mM, pH = 7, T = 25 °C); high resolution XPS spectra of (d) Cu2p3/2 and (e) O1s of CuO@CHFMs before and after reaction; (f) schematic representation of BPA degradation using CuO@CHFMs/PMS system.

feed while the concentration of PMS was reduced to ~0 mM, suggesting that PMS could be completely activated by the CuO coating layer in the presence of excess FFA. According to Fig. 7c in Section 3.4.1, when the initial concentration of PMS was 0.2 mM in the feed, the BPA degradation efficiency also reached to ~94% in the permeate. However, the BPA degradation efficiency was decreased to ~ 6% in the presence of excess FFA and ~0.3 mM PMS in the feed. The results indicated that the inhibition of BPA degradation originated from reactive oxygen species quenching by FFA. Therefore, FFA can be used as the scavenger in the quenching tests. As illustrated in Fig. 10a, the degradation efficiency of BPA was reduced remarkably from 96.3% to 30% when 2 mM FFA was added to the feed. With FFA concentration increased to 10 mM, the BPA removal rate further decreased to ~6%, suggesting BPA oxidation was terminated in the system. Notably, although FFA can react also with $SO_4^{\cdot-}$ and $^{\cdot}OH$, we have verified that $SO_4^{\cdot-}$ and $^{\cdot}OH$ were not the dominant species responsible for BPA degradation in the system. Therefore, the results clearly indicated that $^1O_2$ was generated in the CuO@CHFMs-500-2/PMS system and acted as the dominant oxidative species for the degradation of BPA. Furthermore, electron paramagnetic resonance (EPR) was applied to identify the generation of reactive radicals in the CuO@CHFMs-500-2/PMS system. As shown in Fig. 10b, the characteristic peaks of DMPO-$SO_4^{\cdot-}$ adducts and DMPO-$^{\cdot}OH$ adducts were both detected demonstrating the presence of $SO_4^{\cdot-}$ and $^{\cdot}OH$ in the system. In addition, Fig. 10c clearly reveals a 1:1:1 triplet signal characteristic peaks of TEMP-$^1O_2$, further comfirming that $^1O_2$ was indeed generated in the CuO@CHFMs-500-2/PMS system.

To better understand the activation mechanism of PMS in the system, high resolution XPS spectra of virgin and used CuO@CHFMs were compared. As shown in Fig. 10d, the binding energy (BE) of Cu2p3/2 in fresh CuO@CHFMs was 933.1 eV, implying that Cu(II) was the dominant Cu species. However, the Cu2p3/2 splited into two peaks Cu(II) (932.7 eV) and Cu(I) (934.4 eV) after PMS activation with the relative contents of 50.1% and 49.9%, respectively, indicating that the Cu(II) on the CuO@CHFMs were partially converted to Cu(I) after the catalytic reaction. As shown in Fig. 10e, the O1s peaks at 530.0 eV and

531.3 eV can be interpreted as lattice oxide oxygen (O1) and adsorbed oxygen or surface hydroxyl species (O2). After the reaction, 5.6% of the O2 was transformed to O1, suggestiong adsorbed hydroxyl species might be involved in PMS activation as a ligand in the system [57].

Based on previous studies [9,58,59] and the results discussed above, the possible catalytic mechanism for BPA degradation in the CuO@CHFMs/PMS system is proposed in Fig. 10f, and the main reactions involved in CuO@CHFMs/PMS system can be depicted as follows:

$$Cu(II) + HSO_5^- \rightarrow Cu(I) + SO_5^{\cdot-} + H^+ \tag{2}$$

$$Cu(I) + HSO_5^- \rightarrow Cu(II) + SO_4^{\cdot-} + OH- \tag{3}$$

$$Cu(I) + HSO_5^- \rightarrow Cu(II) + SO_4^{2-} + {}^{\cdot}OH \tag{4}$$

$$2SO_5^{\cdot-} + H_2O \rightarrow 1.5\ {}^1O_2 + 2\ HSO_4- \tag{5}$$

$${}^1O_2 + {}^{\cdot}OH + SO_4^{\cdot-} + BPA \rightarrow intermediates \rightarrow CO_2 + H_2O \tag{6}$$

Firstly, Cu(II) on the surface of CuO@CHFMs is reduced to Cu(I) by PMS (Eq. (2)), and then Cu(I) activates PMS to generate $SO_4^{\cdot-}$ and $^{\cdot}OH$ though Eqs. (3) and (4). Moreover, abundant $^1O_2$ may be produced from the reaction of $SO_5^{\cdot-}$ in the solution via Eq. (5). All the generated ROS (mainly $^1O_2$) then reacted with BPA to accomplish the degradation, as shown in Eq. (6).

To fully understand the degradation process of BPA in the CuO@CHFMs-500-2/PMS system, the main degradation intermediates were detected and identified with UPLC/MS/MS analysis. A total of nine main intermediates were detected for the degradation of BPA in the system. The molecular structure and MS/MS fragmentation information of the oxidation products are displayed in Fig. S5. Based on these degradation intermediates, the possible degradation pathway of BPA is proposed in Fig. 11. As can be seen, the degradation is initiated by β-scission of isopropyl between two phenyl groups in BPA, producing phenol (m/z = 93) and p-isopropyl phenol (m/z = 133). The bond connecting two aromatic rings in BPA is more vulnerable due to the electron-donating hydroxyl group increases the electron density of each aromatic ring [60,61]. The reaction products were further oxidized to
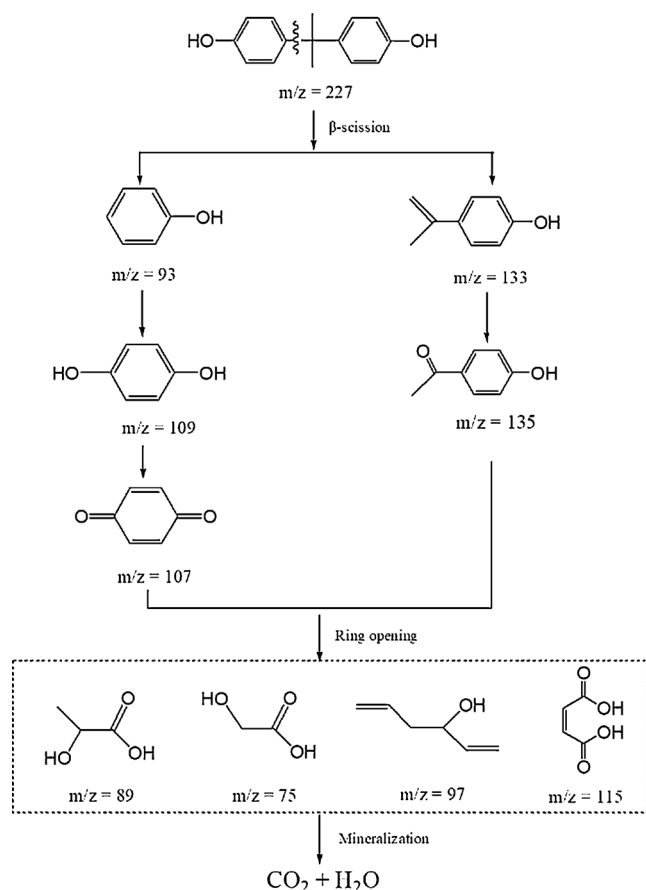
Fig. 11. Proposed degradation pathways of BPA during CuO@CHFMs-500-2/PMS oxidation.

hydroquinone (m/z = 109) and 1-(4-methyl phenyl) ethanone (m/z = 135). Specially, hydroquinone is a well-known instable chemical substance due to its rapid degradation to p-benzoquinone (m/z = 107), while p-benzoquinone cannot be detected, because it is not able to be ionized [26]. The intermediate products were subsequently attacked to form 2-hydroxyacetic (m/z = 75), 2-hydroxypropanoic acid (m/z = 89), 1,5-hexadiene-3-ol (m/z = 97) and maleic acid (m/z = 115).

3.6. Stability and reusability

For a sustainable operation with high performance, it is essential for the CuO@CHFMs to maintain a high catalytic activity and stable structure for prolonged operation time. Therefore, sequential experiments were carried out to investigate the reusability of CuO@CHFMs-

500-2, as shown in Fig. 12a and b. After five cycles, no significant deterioration in the catalytic activity was observed, the degradation rate of BPA and TOC removal efficiency in the system were remained higher than 90% and 50%, respectively. In addition, the leached concentration of Cu ions in the system was ~ 0.1 mg/L in each test and decreased slowly with the increase of cycle times. The leakage of Cu ions in the system is far less than that (1 mg/L) required by environmental quality standards for surface water (GB 3838-2002, China). SEM images in Fig. S6 confirms that the CuO@CHFMs-500-2 maintained huge amounts of CuO particles on the membrane surface after repeated usage. The crystalline structure of CuO taken from the virgin and reused CuO@CHFMs-500-2 was monitored by XRD diffraction pattern and shown in Fig. S7. No apparent change can be identified in the crystalline structure of used CuO in comparison with the virgin sample, indicating the stability of crystal structure for the CuO@CHFMs-500-2 was maintained after repeated using. Further, compared to the employment of CuO catalyst particles with tedious separation processes, the CuO@CHFMs can also address the issue of catalyst separation and recovery, which is of great importance in practical application.

Moreover, the membrane catalytic experiments were also conducted by using the real surface water (Songhuajiang River, China) to investigate the integrated effect of NOM and background ions on the catalytic performance for BPA degradation. The river water quality data and the separation performance of the membrane for the river water were presented in Table S1. As displayed in Fig. 12c, the BPA degradation rate in river water was in close proximity to that obtained in DI water and maintains at a high level of 96.2%, suggesting that the CuO@CHFMs-500-2/PMS system possesses a promising potential for practical application due to the superior membrane separation performance and $^1O_2$ dominated non-radical pathway.

4. Conclusions

In this work, CuO@CHFMs was successfully prepared by combination of phase-inversion, dip-coating and calcination. CuO@CHFMs showed excellent activity and stability in catalytic activation of PMS for BPA oxidation. Benefiting from the dual functionalities of membrane filtration and PMS activation, CuO@CHFMs/PMS system exhibited high resistance to the presence of NOM and high efficiency in the degradation of BPA. A tiny amount of ROS ($SO_4^{\cdot-}$ and $^{\cdot}OH$) were generated in CuO@CHFMs/PMS system, and $^1O_2$ was identified as the main reactive species in this BPA degradation process according to the radical quenching tests and EPR characterization. The $^1O_2$ dominated non-radical oxidation process via PMS activation by CuO@CHFMs overcame the inhibiting effect resulting from the side reaction between radicals and anions (Cl^- and HCO_3^-) in natural waters. This work provides a novel pathway to develop a fascinating strategy incorporating AOPs and membrane process for various applications in water treatment.
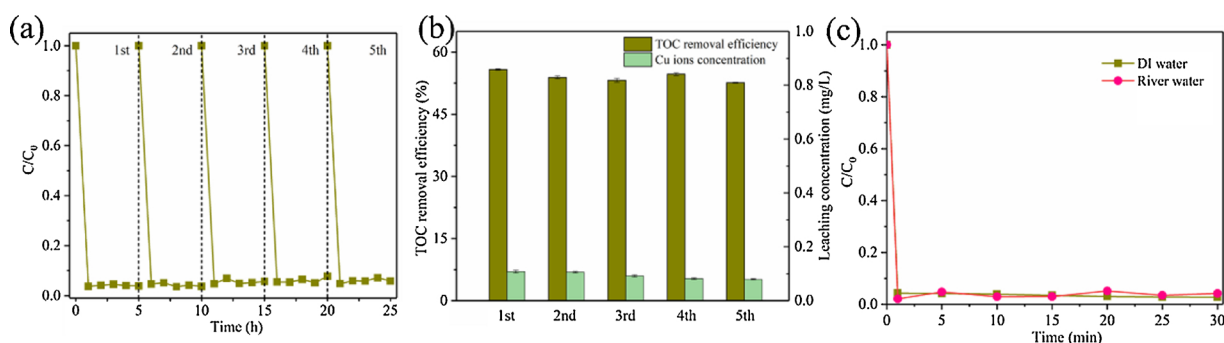

Fig. 12. (a) Reusability test on the CuO@CHFMs-500-2/PMS system for BPA degradation, (b) mineralization of BPA and leached Cu^{2+} concentration in the CuO@CHFMs-500-2/PMS oxidation, (c) effect of water quality on BPA degradation in the CuO@CHFMs-500-2/PMS system ([PMS]$_0$ = 0.5 mM, [BPA]$_0$ = 10 mg/L, Flux = 70 LMH, pH = 7, T = 25 °C).

Acknowledgements

Appendix A. Supplementary data

Supplementary material related to this article can be found, in the online version, at doi:https://doi.org/10.1016/j.apcatb.2019.117783.

References

[1] M. Schulz, A. Soltani, X. Zheng, M. Ernst, J. Membr. Sci. 507 (2016) 154–164.
[2] V.A. Yangali-Quintanilla, A.H. Holm, M. Birkner, S. D´Antonio, H.W.C. Stoltze, M. Ulbricht, X. Zheng, J. Membr. Sci. 499 (2016) 515–525.
[3] F. Gao, J. Wang, H. Zhang, H. Jia, Z. Cui, G. Yang, J. Membr. Sci. 570-571 (2019) 156–167.
[4] L. Song, B. Zhu, V. Jegatheesan, S. Gray, M. Duke, S. Muthukumaran, Environ. Sci. Pollut. Res. Int. 25 (2018) 5191–5202.
[5] J. Xing, H. Wang, X. Cheng, X. Tang, X. Luo, J. Wang, T. Wang, G. Li, H. Liang, Chem. Eng. J. 344 (2018) 62–70.
[6] S.O. Ganiyu, E.D. van Hullebusch, M. Cretin, G. Esposito, M.A. Oturan, Sep. Purif. Technol. 156 (2015) 891–914.
[7] P. Shao, J. Tian, F. Yang, X. Duan, S. Gao, W. Shi, X. Luo, F. Cui, S. Luo, S. Wang, Adv. Funct. Mater. 28 (2018) 1705295.
[8] Z. Zhu, C. Ji, L. Zhong, S. Liu, F. Cui, H. Sun, W. Wang, J. Mater. Chem. A Mater. Energy Sustain. 5 (2017) 18071–18080.
[9] H. Xu, D. Wang, J. Ma, T. Zhang, X. Lu, Z. Chen, Appl. Catal. B: Environ. 238 (2018) 557–567.
[10] M.M. Momeni, Y. Ghayeb, F. Ezati, J. Colloid Interface Sci. 514 (2018) 70–82.
[11] Y.G. Zhang, L.L. Ma, J.L. Li, Y. Yu, Environ. Sci. Technol. 41 (2007) 6264–6269.
[12] J. Tian, C. Wu, H. Yu, S. Gao, G. Li, F. Cui, F. Qu, Water Res. 132 (2018) 190–199.
[13] W.D. Oh, Z. Dong, T.T. Lim, Appl. Catal. B: Environ. 194 (2016) 169–201.
[14] N. Lydakis-Simantiris, D. Riga, E. Katsivela, D. Mantzavinos, N.P. Xekoukoulotakis, Desalination 250 (2010) 351–355.
[15] M. Borges, D. García, T. Hernández, J. Ruiz-Morales, P. Esparza, Catalysts 5 (2015) 77–87.
[16] C. Byrne, G. Subramanian, S.C. Pillai, J. Environ. Chem. Eng. 6 (2018) 3531–3555.
[17] C.P. Athanasekou, N.G. Moustakas, S. Morales-Torres, L.M. Pastrana-Martínez, J.L. Figueiredo, J.L. Faria, A.M.T. Silva, J.M. Dona-Rodriguez, G.E. Romanos, P. Falaras, Appl. Catal. B: Environ. 178 (2015) 12–19.
[18] S. Byun, S.H. Davies, A.L. Alpatova, L.M. Corneal, M.J. Baumann, V.V. Tarabara, S.J. Masten, Water Res. 45 (2011) 163–170.
[19] Y. Yang, H. Wang, J. Li, B. He, T. Wang, S. Liao, Environ. Sci. Technol. 46 (2012) 6815–6821.
[20] Z. Liu, S. Yang, Y. Yuan, J. Xu, Y. Zhu, J. Li, F. Wu, J. Hazard. Mater. 324 (2017) 583–592.
[21] F. Gao, J. Wang, H. Zhang, H. Jia, Z. Cui, G. Yang, J. Membr. Sci. 563 (2018) 592–601.
[22] Q. Wang, Z. Liu, D. Liu, W. Wang, Z. Zhao, F. Cui, G. Li, Chem. Eng. J. 360 (2019) 838–847.
[23] C.-Y. Wang, X. Zhang, H.-B. Qiu, W.-K. Wang, G.-X. Huang, J. Jiang, H.-Q. Yu, Appl. Catal. B: Environ. 200 (2017) 659–665.
[24] S. Hou, L. Ling, D.D. Dionysiou, Y. Wang, J. Huang, K. Guo, X. Li, J. Fang, Environ. Sci. Technol. 52 (2018) 6317–6325.
[25] H. Sun, H. Liu, J. Han, X. Zhang, F. Cheng, Y. Liu, Water Res. 140 (2018) 243–250.
[26] Q. Wang, Z. Liu, D. Liu, G. Liu, M. Yang, F. Cui, W. Wang, Appl. Catal. B: Environ. 236 (2018) 222–232.
[27] Z. Cui, J. Wang, H. Zhang, H.H. Ngo, H. Jia, W. Guo, F. Gao, G. Yang, D. Kang, Bioresour. Technol. 269 (2018) 355–362.
[28] L. Paredes, S. Murgolo, H. Dzinun, M.H. Dzarfan Othman, A.F. Ismail, M. Carballa, G. Mascolo, Appl. Catal. B: Environ. 240 (2019) 9–18.
[29] X. Cheng, H. Liang, F. Qu, A. Ding, H. Chang, B. Liu, X. Tang, D. Wu, G. Li, Chem. Eng. J. 308 (2017) 1010–1020.
[30] T. Zhang, H. Zhu, J.P. Croue, Environ. Sci. Technol. 47 (2013) 2784–2791.
[31] Q. Zhao, D. Lu, H. Jiang, Y. Zhao, Y. Sun, Z. Li, M. Yang, P. Wang, J. Ma, J. Membr. Sci. 573 (2019) 210–217.
[32] P. Shao, J. Tian, X. Duan, Y. Yang, W. Shi, X. Luo, F. Cui, S. Luo, S. Wang, Chem. Eng. J. 359 (2019) 79–87.
[33] X. Duan, H. Sun, J. Kang, Y. Wang, S. Indrawirawan, S. Wang, ACS Catal. 5 (2015) 4629–4636.
[34] H.V. Lutze, N. Kerlin, T.C. Schmidt, Water Res. 72 (2015) 349–360.
[35] Y. Zhou, J. Jiang, Y. Gao, J. Ma, S.Y. Pang, J. Li, X.T. Lu, L.P. Yuan, Environ. Sci. Technol. 49 (2015) 12941–12950.
[36] T. Zhang, Y. Chen, Y. Wang, J. Le Roux, Y. Yang, J.P. Croue, Environ. Sci. Technol. 48 (2014) 5868–5875.
[37] X. Duan, H. Sun, Z. Shao, S. Wang, Appl. Catal. B: Environ. 224 (2018) 973–982.
[38] Y. Bao, T.T. Lim, R. Wang, R.D. Webster, X. Hu, Chem. Eng. J. 343 (2018) 737–747.
[39] K. Ibn Abdul Hamid, P. Sanciolo, S. Gray, M. Duke, S. Muthukumaran, Water Res. 126 (2017) 308–318.
[40] N. Zaouri, L. Gutierrez, L. Dramas, D. Garces, J.P. Croue, Water Res. 116 (2017) 194–202.
[41] S. Wang, J. Tian, Q. Wang, Z. Zhao, F. Cui, G. Li, J. Membr. Sci. 570-571 (2019) 333–342.
[42] E. Adoamnei, J. Mendiola, F. Vela-Soria, M.F. Fernandez, N. Olea, N. Jorgensen, S.H. Swan, A.M. Torres-Cantero, Environ. Res. 161 (2018) 122–128.
[43] P. Shao, Z. Ren, J. Tian, S. Gao, X. Luo, W. Shi, B. Yan, J. Li, F. Cui, Chem. Eng. J. 323 (2017) 64–73.
[44] B. Darsinou, Z. Frontistis, M. Antonopoulou, I. Konstantinou, D. Mantzavinos, Chem. Eng. J. 280 (2015) 623–633.
[45] J. Du, J. Bao, Y. Liu, H. Ling, H. Zheng, S.H. Kim, D.D. Dionysiou, J. Hazard. Mater. 320 (2016) 150–159.
[46] J. Hu, H. Dong, J. Qu, Z. Qiang, Water Res. 112 (2017) 1–8.
[47] L. Zhou, W. Song, Z. Chen, G. Yin, Environ. Sci. Technol. 47 (2013) 3833–3839.
[48] R. Luo, M. Li, C. Wang, M. Zhang, M.A. Nasir Khan, X. Sun, J. Shen, W. Han, L. Wang, J. Li, Water Res. 148 (2019) 416–424.
[49] H. Sun, S. Liu, G. Zhou, H.M. Ang, M.O. Tade, S. Wang, ACS Appl. Mater. Interfaces 4 (2012) 5466–5471.
[50] X. Cheng, H. Guo, Y. Zhang, X. Wu, Y. Liu, Water Res. 113 (2017) 80–88.
[51] E. Saputra, S. Muhammad, H. Sun, H.-M. Ang, M.O. Tadé, S. Wang, Appl. Catal. B: Environ. 154-155 (2014) 246–251.
[52] D. Li, X. Duan, H. Sun, J. Kang, H. Zhang, M.O. Tade, S. Wang, Carbon 115 (2017) 649–658.
[53] P. Liang, C. Zhang, X. Duan, H. Sun, S. Liu, M.O. Tade, S. Wang, Environ. Sci. Nano 4 (2017) 315–324.
[54] C. Qi, X. Liu, J. Ma, C. Lin, X. Li, H. Zhang, Chemosphere 151 (2016) 280–288.
[55] E.T. Yun, J.H. Lee, J. Kim, H.D. Park, J. Lee, Environ. Sci. Technol. 52 (2018) 7032–7042.
[56] S. Zhu, X. Li, J. Kang, X. Duan, S. Wang, Environ. Sci. Technol. 53 (2019) 307–315.
[57] J. Du, J. Bao, Y. Liu, S.H. Kim, D.D. Dionysiou, Chem. Eng. J. (2018), https://doi.org/10.1016/j.cej.2018.05.177.
[58] W. Qin, G. Fang, Y. Wang, D. Zhou, Chem. Eng. J. 348 (2018) 526–534.
[59] F. Guo, K. Wang, J. Lu, J. Chen, X. Dong, D. Xia, A. Zhang, Q. Wang, Chemosphere 218 (2019) 1071–1081.
[60] Q. Han, H. Wang, W. Dong, T. Liu, Y. Yin, H. Fan, Chem. Eng. J. 262 (2015) 34–40.
[61] T. Zhang, Y. Ding, H. Tang, Chem. Eng. J. 264 (2015) 681–689.